11
Water in Nanochannels

Water and its properties in various forms is one of the most actively investigated areas because of its importance in nature. The anomalies that exist in the bulk properties of water make it very interesting and challenging for research, and a vast deal of literature is already available. Even though water has been studied for more than 100 years now, its properties are far from understood. With the advances in fabrication of nanochannels that are only a few molecular diameters in critical dimension, there is now an opportunity for a major breakthrough in understanding the properties of water in confined nanochannels and in validating atomistic simulations. In this chapter, after introducing some definitions and atomistic models for water, we present the static and dynamic behavior of water in confined nanochannels.

11.1 Definitions and Models

Water is composed of two hydrogen atoms and one oxygen atom. Figure 11.1 shows a sketch of the water molecule and the various quantities used to characterize it. For an isolated water molecule (e.g., water in gas phase), it has a *bond length* r_{OH} of 0.95718 Å, and a *bond angle* θ_{HOH} of 104.474°. In the liquid state, both these values are slightly modified by the water−water and/or water−ion interactions. For example, neutron diffraction experiments suggested a bond length of $r_{\mathrm{OH}} = 0.970$ Å and a bond angle of $\theta_{\mathrm{HOH}} = 106.00°$ (Ichikawa et al., 1991) for the liquid state. Because of the higher electronegativity of the oxygen atom compared to that of the

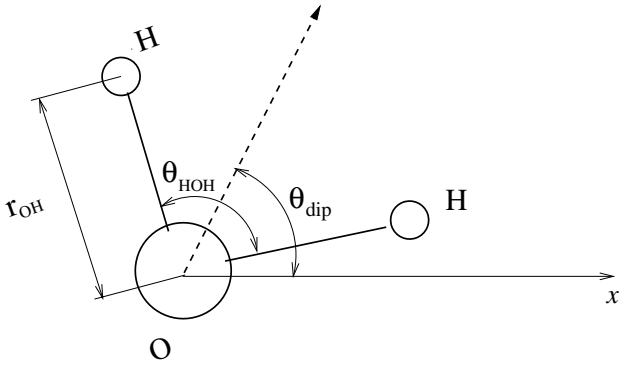

FIGURE 11.1. Sketch of a water molecule and the various quantities used to characterize the water molecule.

hydrogen atom, the oxygen site of the water molecule will appear to be "negatively charged," and the hydrogen site will appear to be "positively charged." Such a charge separation then creates an electric dipole. Because of the symmetry of the water molecule, the dipole can be represented by a line that starts from the oxygen atom and bisects the H−O−H angle (the dotted line in Figure 11.1 is the dipole). If a water molecule is represented by several point charges in an atomistic model, the dipole moment of the model water molecule is given by

$$\boldsymbol{\mu}_{\text{dip}} = \sum_{i=1}^{N} q_i \boldsymbol{r}_i,$$

where N is the number of point charges in the model, and q_i and $\boldsymbol{r}_i$ are the charge and position vector of the point charge i, respectively. The magnitude of the dipole moment, μ_{dip}, is the length of the dipole vector $\boldsymbol{\mu}_{\text{dip}}$. Experimentally, the dipole moment of a single water molecule in liquid state at 300 K is determined to be 2.95±0.2 Debye (1 Debye = 3.336×10^{-30} C m) (Gubskaya and Kusalik, 2002). Sometimes, it is advantageous to describe the water molecule simply as a dipole, e.g., when studying the response of the water molecule to an electrical field. In this case, the orientation of the water is usually characterized by the dipole orientation angle θ_{dip} with respect to a certain reference direction (see Figure 11.1). Some of the important properties of water obtained experimentally are summarized in Table 11.1.

A large number of "hypothetical" models for water have been developed in order to discover the structure of water, on the basis that if the (*known*) model can successfully predict the physical properties of water, then the (*unknown*) structure of water can be determined. They involve positioning the electrostatic sites and Lennard–Jones sites, which may or

TABLE 11.1. Important properties of water (H_2O) †

Dipole moment	2.95 ±0.2 Debye
Boiling point	100°C at 101.325 kPa
Isothermal compressibility	0.4599 GPa^{-1}
Density	997.05 kg/m^3
Dielectric constant	78.4
Diffusion coefficient	$2.27\times10^{-9}m^2/s$
Enthalpy of Vaporization	40.657 kJ/mol (100°)
Electronic polarizability (liquid)	1.48 $Å^3$
Specific heat capacity (C_p)	75.327 J/mol/K
Specific heat capacity (C_v)	74.539 J/mol/K
Thermal conductivity	0.610 W/m/K
Dynamic viscosity	0.8909 mPa·s

†Unless mentioned otherwise, all the properties are reported at 25° C.

may not coincide with one or more of the charged sites. Generally, each model is developed to match well a certain set of physical structures or parameters (e.g., the density anomaly, radial distribution function, or other critical parameters). A discussion of the various atomistic models for water is presented next.

11.1.1 Atomistic Models

There are a number of atomistic models for water, and a description of the majority of the models can be found in (Chaplin, 2004). In this section we summarize only the most commonly used models for water.

The SSD Model

The water molecule in the soft sticky dipole (SSD) model is treated as a Lennard–Jones sphere with an embedded point dipole plus a tetrahedral "sticky" potential, all situated at the molecular center of mass (M) located on the H-O-H bisector at 0.0654 Å from the oxygen toward the hydrogens (see Figure 11.2). The geometry of the water molecule used in this model is similar to that of any three-site model (e.g., TIP3P). The O-H length (i.e. r_{OH}) is 0.9572 Å and the H-O-H angle (i.e. θ_{HOH}) is 104.52°. The H-M-H angle is 109.47°. The center of mass is the only interaction site of this model (Liu and Ichiye, 1996).

In the SSD model, the total interaction potential energy between two water molecules i and j is given by (Liu and Ichiye, 1996)

$$V_{ij} = V_{ij}^{LJ}(r_{ij}) + V_{ij}^{dp}(\mathbf{r}_{ij}, \Omega_i, \Omega_j) + V_{ij}^{sp}(\mathbf{r}_{ij}, \Omega_i, \Omega_j), \tag{11.1}$$

where r_{ij} is the distance between the molecular centers, $\mathbf{r}_{ij}$ is the separation vector between two molecular centers, and Ω is the orientation of the water

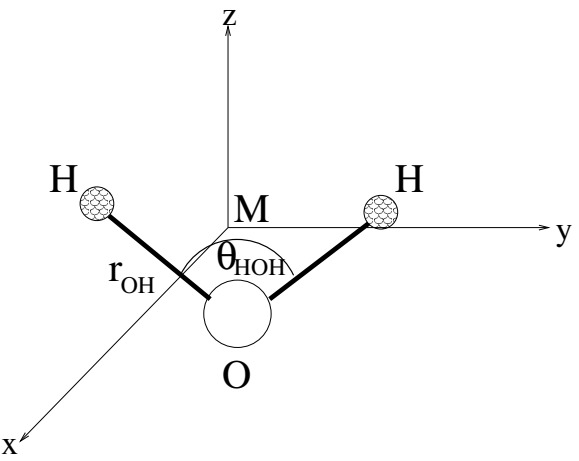

FIGURE 11.2. Schematic representation of a three-site water model. This particular model corresponds to the geometry of SSD. M is the molecular center of mass, which is taken as the origin.

molecule, which is determined by both the orientation of the dipole moment vector and the orientation of the molecular plane. The first term in equation (11.1) is the Lennard–Jones potential (see Section 16.1 for more details),

$$V_{ij}^{LJ}(r_{ij}) = 4\epsilon_w \left[\left(\frac{\sigma_w}{r_{ij}} \right)^{12} - \left(\frac{\sigma_w}{r_{ij}} \right)^{6} \right],$$

where $\sigma_w = 3.051$ Å and $\epsilon_w = 0.152$ kcal/mol (Liu and Ichiye, 1996). The second term in equation (11.1) is the point dipole–point dipole potential,

$$V_{ij}^{dp}(\mathbf{r}_{ij}, \Omega_i, \Omega_j) = \frac{\boldsymbol{\mu}_i \cdot \boldsymbol{\mu}_j}{r_{ij}^3} - \frac{3(\boldsymbol{\mu}_i \cdot \mathbf{r}_{ij})(\boldsymbol{\mu}_j \cdot \mathbf{r}_{ij})}{r_{ij}^5},$$

where $\boldsymbol{\mu}_i$ and $\boldsymbol{\mu}_j$ are the dipole moment vectors, each of whose magnitude is 2.35 D. Note that the factor $1/4\pi\epsilon_0$ has been omitted for simplicity in defining the potential due to electrostatic charges. The last term in equation (11.1) is the tetrahedral sticky potential,

$$V_{ij}^{sp}(\mathbf{r}_{ij}, \Omega_i, \Omega_j) = V^\circ \left[s(r_{ij}) w_{ij}(\mathbf{r}_{ij}, \Omega_i, \Omega_j) + s'(r_{ij}) w_{ij}^x(\theta_{ij}) \right],$$

where $V^\circ = 3.7284$ kcal/mol determines the strength of the sticky potential. The function $w_{ij}(\mathbf{r}_{ij}, \Omega_i, \Omega_j)$ is given by

$$w_{ij}(\mathbf{r}_{ij}, \Omega_i, \Omega_j) = \sin(\theta_{ij}) \sin(2\theta_{ij}) \cos(2\varphi_{ij}) + \sin(\theta_{ji}) \sin(2\theta_{ji}) \cos(2\varphi_{ji}),$$

where $(\theta_{ij}, \varphi_{ij})$ is the set of spherical polar angles of the position of molecule j in the frame fixed on molecule i and with an orientation such that the

Z-axis is parallel to the dipole moment of i and the X-axis is perpendicular to the molecular plane of i. In addition, $w_{ij}^{x}(\theta_{ij})$ is an empirical correction form added to the sticky potential; $s(r_{ij})$ and $s'(r_{ij})$ are the modulating functions, which interpolate between 0 and 1. The properties of water modeled by SSD are given in Table 11.3.

Evaluation of the interaction between two SSD water molecules requires computing only one distance between the two centers of mass, four spherical angles, and the angle between the dipole vectors. On the other hand, three-site models like TIP3P and SPC/E require computing nine intermolecular distances, while five-site models like ST2 and TIP5P require computing 17 intermolecular distances. Simulations with the SSD potential are about 4 times and 7 times faster compared with the three-site models in molecular dynamics (Tan et al., 2003) and Monte Carlo (Tan et al., 2003), respectively. The original parameters of the SSD water model give low water density (0.977 g/cm^3) and low heat of vaporization energy at room temperature and 1 atmosphere. However, these issues have been addressed by (Tan et al., 2003) by optimizing the parameters used in the SSD potential.

The SPC Model

The simple point charge (SPC) model is also a three-site model. It consists of a tetrahedral water model with an OH distance of 0.1 nm, H-O-H angle of 109.47°, point charges on the oxygen and hydrogen positions of $-0.82e$ and $+0.41e$ (electronic charge units), respectively, and a Lennard–Jones interaction on the oxygen positions given by

$$V_{\mathrm{LJ}} = -(A/r)^6 + (B/r)^{12}, \tag{11.2}$$

where $A = 0.37122$ (kJ/mol)$^{1/6}\cdot$ nm and $B = 0.3428$ (kJ/mol)$^{1/12}\cdot$ nm. The total interaction energy between two SPC water molecules consists of the Lennard–Jones potential and the Coulombic potential based on classical electrostatics,

$$V_{\mathrm{total}} = V_{\mathrm{LJ}} + V_C, \tag{11.3}$$

where V_C between two molecules i and j is represented as the sum of Coulomb interactions acting among the charged points (i.e., the O and H atoms' positions) in the following way:

$$V_C = \sum_{\mathrm{O,H}} \frac{q_I q_J}{r_{ij}^{IJ}}, \tag{11.4}$$

where r_{ij}^{IJ} is the distance between site I of the molecule i and site J of the molecule j.

The geometry is similar to the water geometry shown in Figure 11.2. However, the center of mass coincides with the oxygen atom for the SPC model. The dipole moment of the SPC model is 2.27 D, compared to 1.85 D for the isolated molecule. The diffusion coefficient of the model is 3.6×10^{-5}

$cm^2 \cdot s^{-1}$ at 300 K. The potential energy for liquid SPC water (Berendsen et al., 1987) at 300 K is −41.7 kJ/mol, and the density at 300 K and atmospheric pressure turns out to be $0.98\ g \cdot cm^{-3}$. Although the model behaves quite satisfactorily for most purposes, there is room for improvement with respect to density, radial distribution function, and diffusion constant. The properties of the SPC model are summarized in Table 11.3.

The SPC/E Model

The extended simple point charge (SPC/E) model is characterized by three point masses with O-H distance of 0.1 nm, H-O-H angle equal to 109.47°, charges on the oxygen and hydrogen equal to −0.8476 e and +0.4238 e, respectively, and with Lennard–Jones parameters of oxygen–oxygen interaction according to equation (11.2) ($A = 0.37122$ $(kJ/mol)^{1/6} \cdot$ nm and $B = 0.3428$ $(kJ/mol)^{1/12} \cdot$ nm) (Berendsen et al., 1987). The interaction between two SPC/E water molecules is represented by equations (11.2), (11.3) and (11.4). The SPC/E model has a dipole moment of 2.35 D. The diffusion constant is improved considerably compared to the SPC model. The agreement of the radial density distribution with experiment is somewhat better for the SPC/E model than for the SPC model (Berendsen et al., 1987).

The ST2 model

The ST2 potential developed by (Stillinger and Rahman, 1974) is based on a rigid four-point-charge model for each water molecule. The ST2 water model is shown in Figure 11.3. The positive charges $+q$ are identified as partially shielded protons, and they have been located precisely 1 Å from the oxygen nucleus, O. The distance l from O to each of the negative charges $-q$ is 0.8 Å in the ST2 model. Pairs of vectors connecting O to the point charges are all disposed at an angle θ_t,

$$\theta_t = 2\cos^{-1}(3^{-1/2}) \approx 109°28'.$$

The ST2 molecules interact with each other through a potential function consisting of a Lennard–Jones central potential acting between oxygens, plus a Coulombic potential for the 16 (4×4) pairs of point charges. The ST2 model has a dipole moment of 2.353 D (Stillinger and Rahman, 1974).

The TIPnP Model

The geometry of the TIP5P model is shown in Figure 11.4, and its parameters are presented in Table 11.2, along with those for the TIP3P and TIP4P models. For all TIPnP models, the O-H bond length r_{OH} and H-O-H bond angle θ_{HOH} have been set to the experimental gas-phase values, i.e., 0.9572 Å and 104.52°. For TIP5P, the negatively charged interaction sites are located symmetrically along the lone-pair directions with an intervening

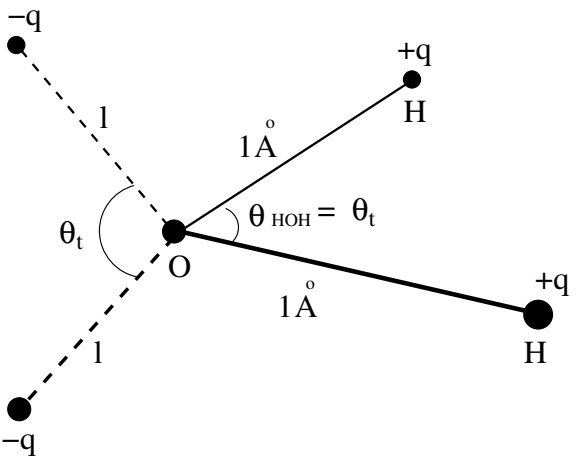

FIGURE 11.3. A sketch of an ST2 water model.

angle, θ_{LOL} , of 109.47°. A charge of +0.241 e is placed on each hydrogen site, and charges of equal magnitude and opposite sign are placed on the lone-pair interaction sites. The dipole moments are 2.35 D, 2.18 D, and 2.29 D for TIP3P, TIP4P, and TIP5P, respectively. There is no charge on oxygen for TIP5P. The Lennard–Jones potential acts on only the oxygens with a σ_0 of 3.12 Å and an ϵ_0 of 0.16 kcal/mol. The potential energy between two water molecules a and b is then given by the following equation (Mahoney and Jorgensen, 2000):

$$V_{ab} = \sum_{ij} \frac{q_i q_j e^2}{r_{ij}} + 4\epsilon_0 \left[\left(\frac{\sigma_0}{r_{\mathrm{OO}}} \right)^{12} - \left(\frac{\sigma_0}{r_{\mathrm{OO}}} \right)^{6} \right], \tag{11.5}$$

where i and j are the charged sites on a and b, respectively, and r_{OO} is the oxygen–oxygen distance.

The geometry of the TIP4P water model is shown in Figure 11.5. The TIP4P model is based on four interaction sites located in a planar configuration. Two of those are labeled M and O, which are associated with the oxygen nucleus, and the other two (which are labeled H) are the protons. The two distances and one angle required to fully specify the site coordinates are $r_{\mathrm{OH}} = 0.957$ Å, $r_{\mathrm{OM}} = 0.15$ Å (M lies on the axis of symmetry between O and the line joining the H sites), and $\measuredangle \mathrm{HOH} = 104.5°$.

The potential energy between two TIP4P water molecules consists of a double sum over the interaction sites of both molecules; the terms in the sum allow for Coulombic interactions between the electric charges assigned to the sites as well as an LJ-type contribution (equation (11.5)). The charge on the H site is equal to $0.52e$, on the oxygen site is zero, and on the M site is equal to $-1.04e$ (Rapaport, 1997). The physical properties of water based

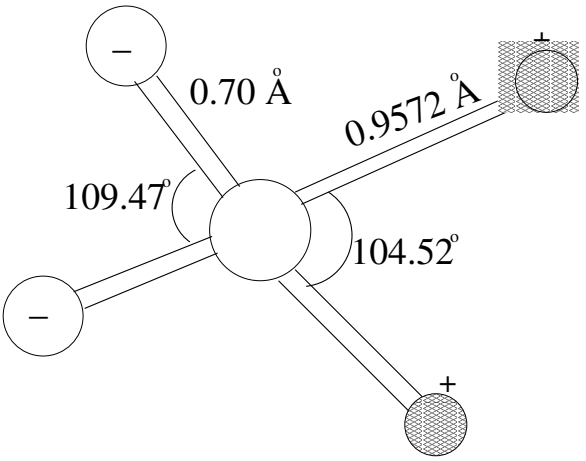

FIGURE 11.4. A sketch of the TIP5P monomer geometry.

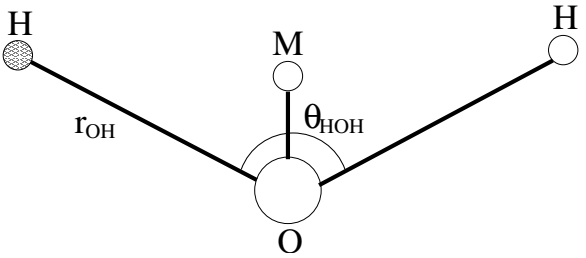

FIGURE 11.5. A sketch of the planar TIP4P water molecule.

on the TIP4P model are summarized in Table 11.3, and the geometrical and interaction parameters of the TIP4P model are summarized in Table 11.2.

The PPC Model

The polarizable point charge (PPC) model is an efficient polarizable model that retains most of the simplicity of the popular classical three-site potentials while incorporating the polarization response of the water molecule to a local electric field as determined from ab initio calculations (Svishchev et al., 1996). Studies (Kusalik et al., 1995) have shown that the PPC potential accurately describes both the virial equation of state for steam and the liquid properties, including the local structure, dielectric constant, the self-diffusion coefficient, and the Debye relaxation time (Kusalik et al., 1995), over a wide range of temperatures. The distance between O and H (i.e., r_{OH}) in the PPC model is equal to 0.943 Å and $\measuredangle\mathrm{HOH} = 106°$. The ge-

TABLE 11.2. Monomer geometry and parameters for the TIPnP potential functions (Mahoney and Jorgensen, 2000).

Parameters	TIP3P	TIP4P	TIP5P
q_{H} (e)	0.417	0.520	0.241
σ_0 (Å)	3.15061	3.15365	3.12
ϵ_0 (kcal/mol)	0.1521	0.1550	0.16
r_{OH} (Å)	0.9572	0.9572	0.9572
θ_{HOH} (deg)	104.52	104.52	104.52
r_{OL} (Å)	–	0.15	0.70
θ_{LOL} (deg)	–	–	109.47

ometry of the PPC water model is similar to the geometry of the three-site water model shown in Figure 11.2. The values of the hydrogen charges are given by (Kusalik et al., 1995)

$$q_+ = 0.486 \pm 0.03E_x + 0.02E_z,$$

where for the second term a "+" sign is used for one of the hydrogens and a "−" sign is used for the other hydrogen, and the electric field is given in V/Å. The charge on the negative site follows from charge neutrality. The short-range interaction of the PPC model is taken to be an LJ potential centered on the oxygen. The LJ parameters, $\epsilon_{\mathrm{LJ}} = 0.6$ kJ/mol and $\sigma = 3.234$ Å, are optimized to give the correct energy, self-diffusion coefficient, and structure for water at 25°C. It is observed by (Kusalik et al., 1995) that unlike other polarizable models, which typically execute at least three times slower than effective potential models, a comparable calculation with the PPC model runs only 1.5 times slower than a simulation with SPC/E water. The physical properties of the water simulated using the PPC model are summarized in Table 11.3.

The Six-Site Model

(Nada and van der Eerden, 2003) have proposed an intermolecular potential model of a rigid H_2O molecule that has six interaction sites. It has been observed that this six-site model is much more suitable for the simulation of ice and water near T_{M} (i.e., melting point of ice) than the TIP4P and TIP5P models. Figure 11.6 shows a sketch of the six-site model. A positive point charge is placed on each hydrogen (H) site, and a negative charge on each lone-pair (L) site, as in the TIP5P model. A negative charge is also placed on a site M, which is located on the bisector of ∡HOH, as in the TIP4P model. In contrast to the TIP4P and TIP5P models, the Lennard–Jones interaction acts not only on the oxygen (O) site but also on the H sites in the present model. For the O-H length (r_{OH}) and H-O-H angle in this model, intermediate values between those of the real molecule

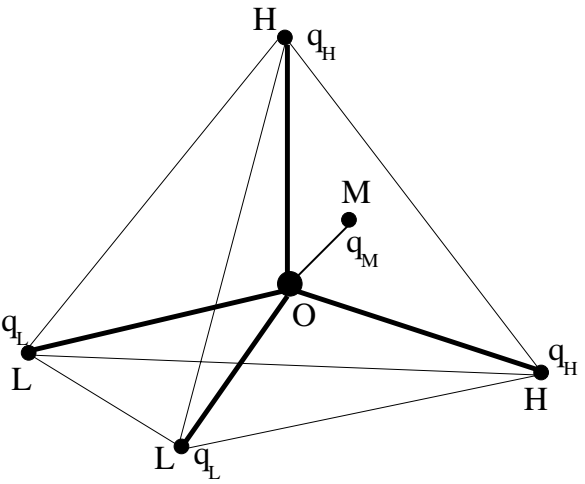

FIGURE 11.6. Schematic illustration of the water molecule in the six site model.

in the ice and vapor phases are taken (Nada and van der Eerden, 2003). The average of ∠HOH and ∠LOL in the present model is the tetrahedral angle of 109.5°. The intermolecular interaction between molecules i and j, V_{ij}, is represented as the sum of the Coulomb interactions acting among the charged points and the Lennard–Jones interactions acting on O and H atoms, in the following way:

$$V_{ij} = \sum_{\mathrm{H,L,M}} \frac{q_I q_J}{r_{ij}^{IJ}} + 4 \sum_{\mathrm{O,H}} \epsilon_{IJ} \left[\left(\frac{\sigma_{IJ}}{r_{ij}^{IJ}} \right)^{12} - \left(\frac{\sigma_{IJ}}{r_{ij}^{IJ}} \right)^{6} \right],$$

where r_{ij}^{IJ} is the distance between site I of the molecule i and site J of molecule j. Here q_I (see Figure 11.6) gives the charge amount of site I.

Summary of Physical Properties

Table 11.3 summarizes some of the important properties of water obtained from various water models.

11.2 Static Behavior

The static behavior of water in various confined states—near a surface, in a slit pore, or in a cylindrical pore—is discussed in this section. The static behavior includes density distribution, dipole orientation, hydrogen bonding and clustering, and the contact angle of water to the surface in a nano-confinement environment. These properties are of fundamental interest and of critical importance. For example, an understanding of the

TABLE 11.3. Some of the calculated physical properties of the water models †

Model	μ_{dip} (Debye)	ϵ (relative)	D_{self} (10^{-5} cm^2/s)	E_{config} (kJ/mol)	T_{max} (°C)
SSD	2.35	72	2.13	-40.2	-13
SPC	2.27	65	3.85	-41.0	–
SPC/E	2.35	71	2.49	-41.5	-38
PPC	2.52	77	2.60	-43.2	+4
TIP3P	2.35	82	5.19	-41.1	-13
TIP4P	2.18	53*	3.29	-41.8	-25
TIP5P	2.29	81.5	2.62	-41.3	+4
six-site	1.89	33	–	–	+14
Expt.	2.65, 3.0	78.4	2.30	-41.5	+3.98

†Note that μ_{dip}, ϵ, D_{self}, E_{config}, and T_{max} denote the dipole moment, dielectric constant, self diffusion coefficient, average configurational energy, and maximum density temperature. All the data are at 25° and 1 atm, except * at 20°.

density distribution and dipole orientation of the water molecules near a surface is crucial for understanding the electrochemical reaction at a surface (Henderson et al., 2001). In recent years, experimental techniques have improved dramatically, and it is now possible to probe the structure of a liquid at atomistic detail (Toney et al., 1994; Cheng et al., 2001). For example, based on x-ray scattering measurements, (Toney et al., 1994) have proposed that water is ordered in layers extended to about three molecular diameters from an electrode surface and that water density near a charged electrode is very high. Though these experiments can provide good insight into water density distribution and dipole orientation, they cannot provide detailed and direct information of these functions; rather, they provide information about the integrals involving these functions. In addition, these experiments can probe only relatively simple geometry and cannot be used easily to study how the various parameters (e.g., surface characteristics) influence the static behavior of water in confined states. To this end, atomistic simulations have been more sucessfully used, and we will review some of the interesting results here.

11.2.1 Density Distribution and Dipole Orientation

There is an extensive literature on the density distribution and dipole orientation of water near a one-dimensional surface (Henderson et al., 2001; Yeh and Berkowitz, 2000; Spohr et al., 1998; Galle and Vortler, 1999; Gordillo and Martí, 2003; Puibasset and Pellenq, 2003; Muller and Bubbins, 1998) (1-D confinement), inside a cylindrical pore (Henderson et al., 2001; Allen et al., 1999; Rovere and Gallo, 2003; Walther et al., 2001a; Allen et al., 2002;

Gallo et al., 2000; Lynden-Bell and Rasaiah, 1996; Leo and Maranon, 2003; Gallo et al., 2002a; Gallo et al., 2002b; Green and Lu, 1997) (2-D confinement) and inside a cavity (Levinger, 2002; Brovchenko et al., 2001; Egorov and Brodskaya, 2003) (3-D confinement). Here we focus on how the density and the dipole orientation of the water molecules are influenced by the degree of confinement (e.g., size of nanopore), by the properties of surface (e.g., hydrophobic vs. hydrophilic surface), and by the presence of surface charge.

(Allen et al., 1999) studied the water density and the dipole orientation in a cylindrical pore systematically by varying the pore size and the surface properties. Three types of pores were considered. The first is a hydrophobic wall consisting of a regular array of Lennard–Jones (LJ) 12-6 centers on a cylindrical shell; the second is a structureless one-dimensional potential function that approximates the atomic hydrophobic wall; and the third is a hydrophilic surface containing an array of bound water molecules. Figure 11.7 shows the water oxygen atom density profiles against distance from the effective wall radius for each surface type and for an effective radius $R =$ 2.1 Å to 5.6 Å. The pore is solvated by a band of water molecules centered at 1.2 to 1.4 Å from the effective channel radius. The hydrophobic and hydrophilic channels result in very different water density profiles. Inside hydrophobic channels, for $R \leq 3.6$ Å, there is only one layer of water, while there are two layers for larger cross-sections. In a hydrophilic channel, the water molecules are able to approach closer to the channel wall, resulting in a more sharply defined density peak compared to that in a hydrophobic channel. The location of the first water density peak near the channel wall is also shifted toward the channel wall for the hydrophilic surface case. In addition, in large pores, a third peak of water density appears when the channel surface is hydrophilic.

Figure 11.8 shows 20-Å segments of the center of mass corrected water oxygen atom density profiles along the channel axis (z-direction) for atomic hydrophobic (A), LJ hydrophobic (B), and hydrophilic channels (C) with $R = 2.6$ Å, 4.1 Å, and 5.6 Å. Note that for both hydrophobic channels, a transition occurs at $R = 4.1$ Å, where the water becomes highly structured, and well-defined layers emerge. The similar results for the two hydrophobic channels suggest that an explicit treatment of the atomic structure of the channel does not have an appreciable effect on water structure. Hence, the atomic hydrophobic channels are well represented by a one-dimensional potential function. The LJ 5-3 function can be used to significantly reduce the simulation times, since this gives a good reproduction of structural properties of water. In the hydrophilic channels, the water structure exhibits a markedly different behavior, with only the narrow 2.6-Å channel exhibiting some order along the channel axis.

Figure 11.9 shows the dipole orientation distribution for channels of effective radius 2.6 Å (panel A), 4.1 Å (panel B) and 5.6 Å (panel C). The left panels show the average projection of dipole orientation onto the z-

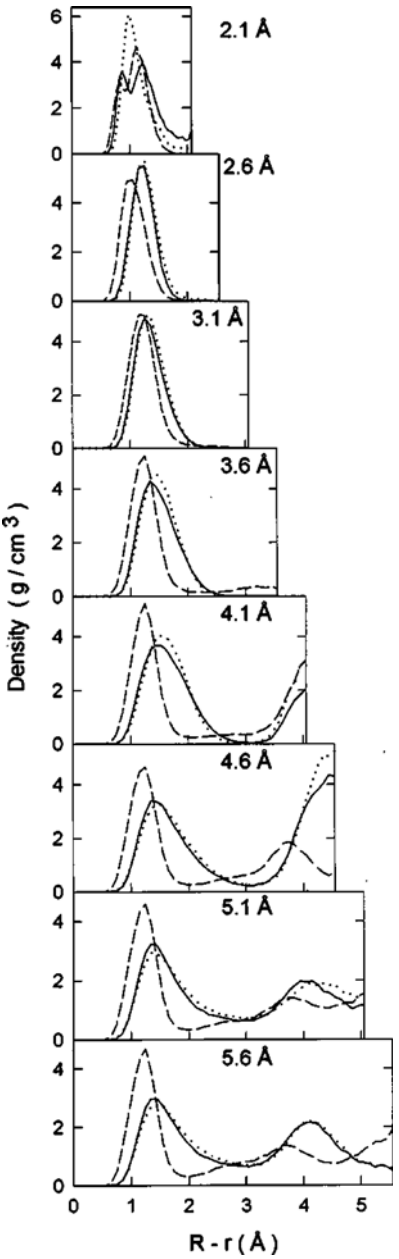

FIGURE 11.7. Water–oxygen atom radial density profiles: Density profiles for the atomic hydrophobic (solid curve), LJ hydrophobic (dotted curve), and hydrophilic (dashed curve) channels are compared for effective channel radii 2.1–5.6 Å. All profiles are plotted against the distance from the effective wall, of the channel $R-r$. The left-hand vertical axis represents the effective wall, while the right-hand axis represents the channel axis z. Each graph is labeled with the effective channel radius R. (Courtesy of S.-H. Chung.)

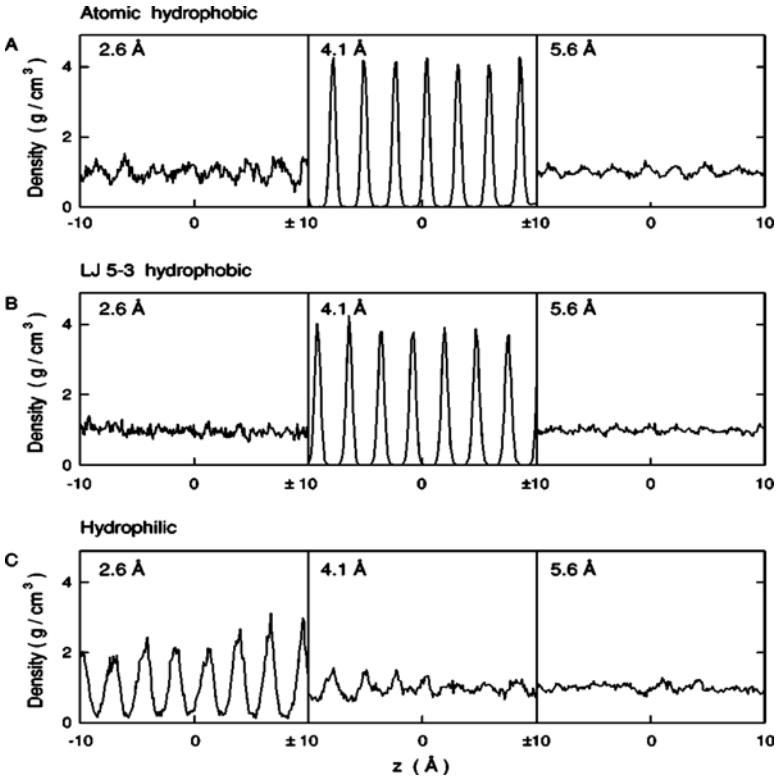

FIGURE 11.8. Water–oxygen atom density profiles along the channel axis direction: (A) Density profile for atomic hydrophobic channels of effective radii 2.6 Å (left panel), 4.1 Å (central panel), and 5.6 Å (right panel). (B) Density profiles for LJ hydrophobic surface described by the LJ 5-3 potential. (C) Density profiles for hydrophilic channels. (Courtesy of S.-H. Chung.)

direction (channel axis direction) for atomic hydrophobic (solid curve), LJ hydrophobic (dotted curve), and hydrophilic (dashed curve) channels. The right panels show the projection onto the radial vector $\mathbf{r}$. In the hydrophobic channels, water molecules have a definite preference to point either up or down the channel axes, and such a trend is especially clear in narrow channels. Most distributions possess symmetry about the origin and result in zero net dipole moment. However, in a very narrow channel (e.g., $r =$ 2.6 Å), the symmetry is broken, and this leads to a rather large net dipole moment along the channel. In contrast, in the hydrophilic channels, the water dipoles prefer to lie in the xy-plane rather than align along the channel axis, and align themselves more toward the channel wall. The net dipole moments are zero in all the hydrophilic channels. Clearly, the geometrical confinement alters the behavior of water from that in the bulk, and the effects of different types of surfaces make its behavior further complicated.

This can have a very profound influence on various macroscopic measurables. As discussed by (Allen et al., 1999), an ion attempting to pass along a line of dipoles aligned head to tail (as in the narrow hydrophobic channel case) will be impeded less than if it were to pass alongside a line of dipoles oriented perpendicular to the line (as in a hydrophilic channel), and this can lead to very different transport behavior of the ions.

Density distribution and dipole orientation studies have also been performed on charged nanopores. (Hartnig et al., 1998) studied the density distribution and dipole orientation of water molecules in two cylindrical nanopores with a radius of 10.9 Å. In the first pore, there are 72 alternating positive and negative elementary charges on the pore surface, and the second pore has no surface charge. Figure 11.10 shows the oxygen and hydrogen density distribution for the two pores. From the graph, we observe that the water oxygen density has a slightly larger peak when the pore is charged. In addition, the density peak of the oxygen atoms is closer to the pore surface when the nanopore is charged. This can be explained by the attraction of the water molecules toward the nanopore surface. The hydrogen atom density profile shows a peak at $R = 9.2$ Å, which was not observed when the pore was not charged. This is caused by the attraction of the hydrogen atoms by the negative surface charges, which is not balanced by the short-range Lennard–Jones repulsion as in the case of oxygen. Figure 11.11 shows the average dipole moment of a water molecule in the radial direction as a function of its radial position. For both charged and noncharged pores, we observe that the water dipole tends to point toward the pore center in the region 6.7 Å $< R < 7.2$ Å (where R is the pore radius). However, in the charged pore, there is an additional region $R > 8.2$ Å, where the dipoles point toward the pore surface, consistent with the hump in the hydrogen density profile at $R = 9.2$ Å. From these results, we can conclude that the presence of a charge on the pore surface can influence the density distribution, dipole orientation, and the average dipole moment.

Water confined in silica pores has also been investigated. Silica and other porous materials are of great interest for a number of nanotechnology applications including catalytic and separation processes. (Gallo et al., 2000) have examined the density profiles of water confined in a cylindrical Vycor glass pore at various hydration levels (the smaller the number of water molecules in the pore, the smaller the hydration level). Figure 11.12 shows the snapshot of equilibrium configuration of confined water at various hydration levels (the pore diameter is 4.0 nm). The hydrophilic nature of the Vycor glass is evident, since all the water molecules are attracted toward the pore surface. Low amounts of water (e.g., the number of water molecules is 500) are almost completely adsorbed on the pore surface. With increasing water concentration, water molecules occupy an increasing fraction of the free volume of the pore. For about 2600 water molecules, the hydration level is found to be close to 100%.

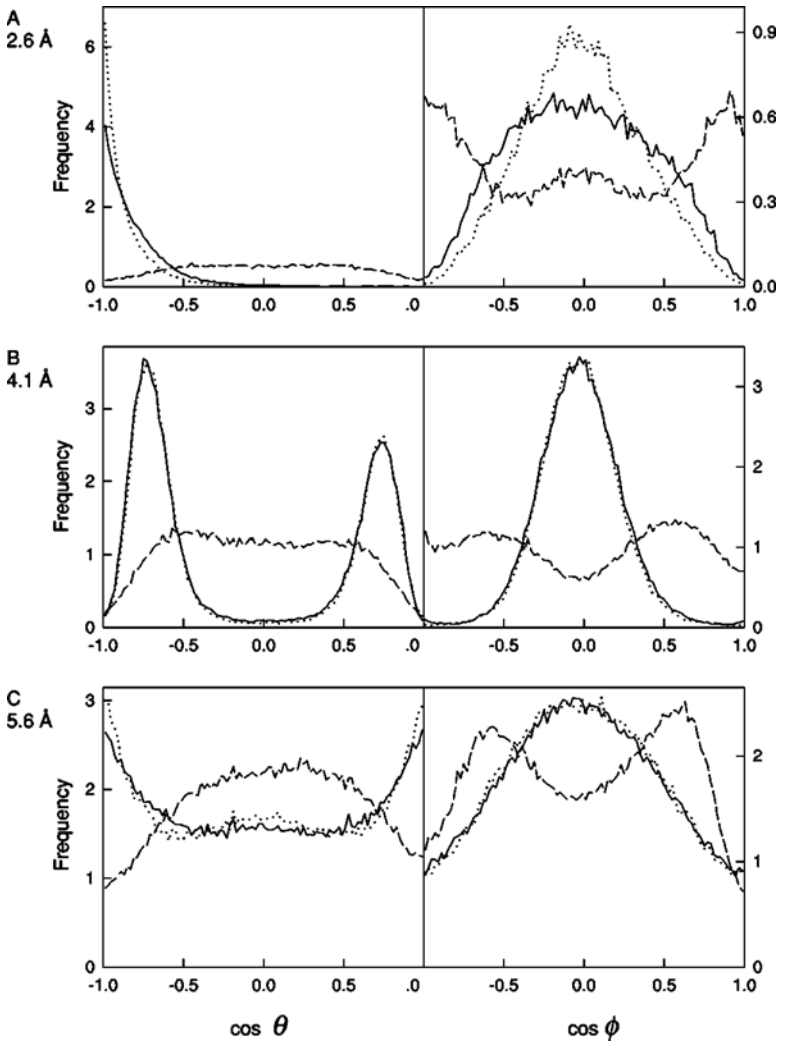

FIGURE 11.9. Water dipole orientation distributions for channels of effective radius 2.6 Å (A), 4.1 Å (B), and 5.6 Å (C). The left panels show the average projection of dipole orientation onto the z-axis ($\cos(\theta)$) for atomic hydrophobic (solid curve), LJ hydrophobic (dotted curve), and hydrophilic (dashed curve) channels. The right panels show the projections of the dipole onto the radial vector $\mathbf{r}$ ($\cos(\phi)$). (Courtesy of S.-H. Chung.)

11.2.2 Hydrogen Bonding

A hydrogen atom covalently bound to an electronegative atom (e.g., nitrogen, oxygen) has a significant positive charge and can form a weak bond

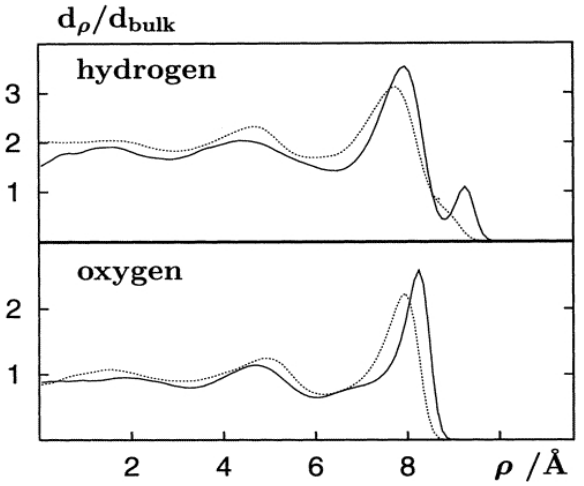

FIGURE 11.10. Oxygen and hydrogen density distribution in a cylindrical pore of radius 10.9 Å (ρ denotes the radius of the pore in Å) when the pore wall has alternating positive and negative elementary charges (solid line) and when the pore wall has no charges (dotted line). (Courtesy of E. Sphor.)

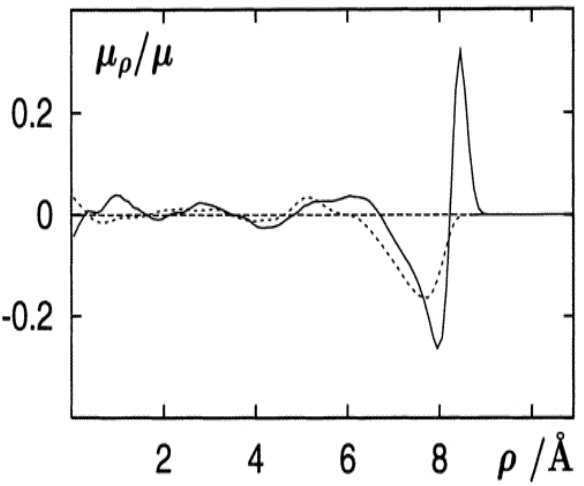

FIGURE 11.11. Average dipole moment (divided by the molecular dipole of TIP4P water model) as a function of the radial position (ρ) in the pore. Solid line: charged pore wall. Dotted line: uncharged pore wall. (Courtesy of E. Spohr.)

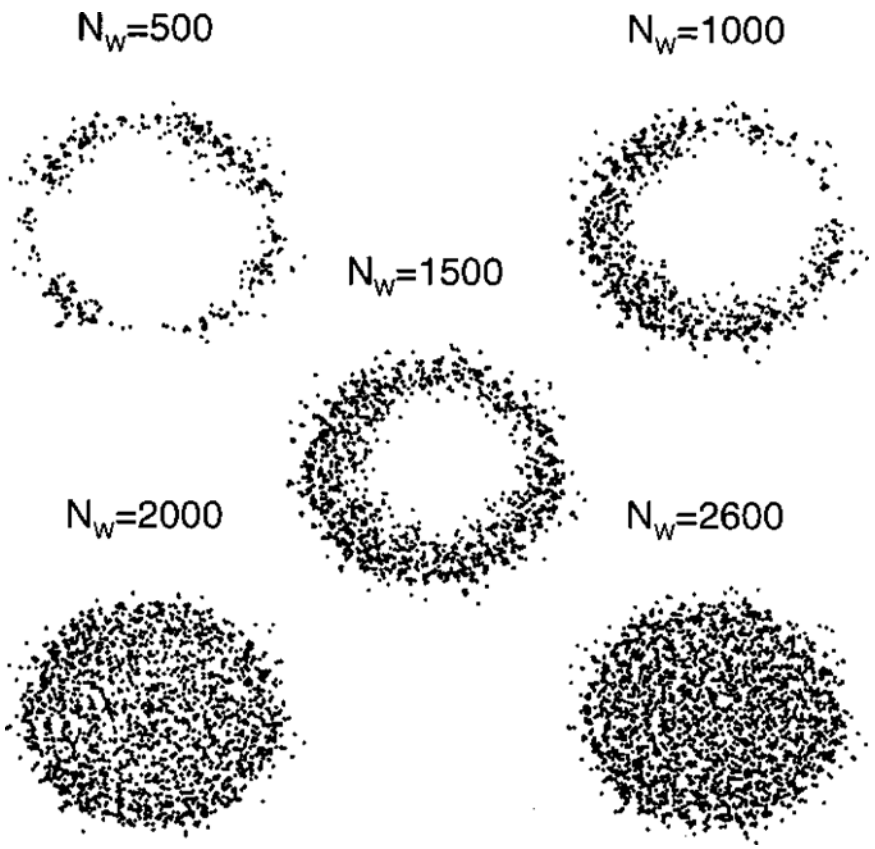

FIGURE 11.12. Snapshots of equilibrium configuration of confined water at different hydration levels. Only the oxygen atoms of water are shown projected on the xy-plane perpendicular to the axis of the confining cylinder. N_w is the number of water molecules in the pore. $N_w = 500$, 1000, 1500, 2000, and 2600 correspond to approximately 20%, 40%, 60%, 75%, and 100% hydration levels. (Courtesy of M. Rovere.)

to another electronegative atom, and such a bond is usually termed as a hydrogen bond. Water molecules in liquid state can form an extensive hydrogen bonding network. Figure 11.13 shows the scenario of hydrogen bonding between two water molecules. The strength of hydrogen bonds ($\approx$ 21 kJ/mol) is normally intermediate between that of the weak van der Waals interactions ($\approx$ 1.25 kJ/mol) and that of the covalent chemical bonds ($\approx$ 420 kJ/mol).

In atomistic simulations, there are two types of criteria for determining whether two water molecules form a hydrogen bond, namely, an energetic criterion and a geometric criterion. In the energetic criterion, two water

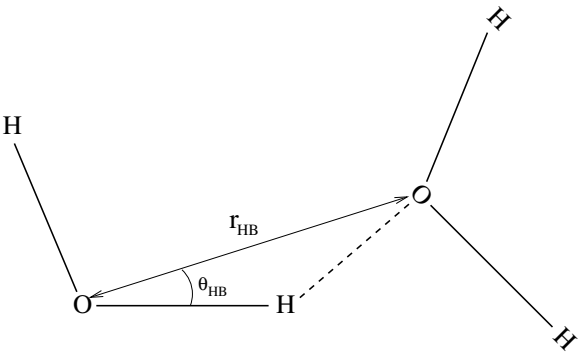

FIGURE 11.13. Schematic of the hydrogen bonding between two water molecules.

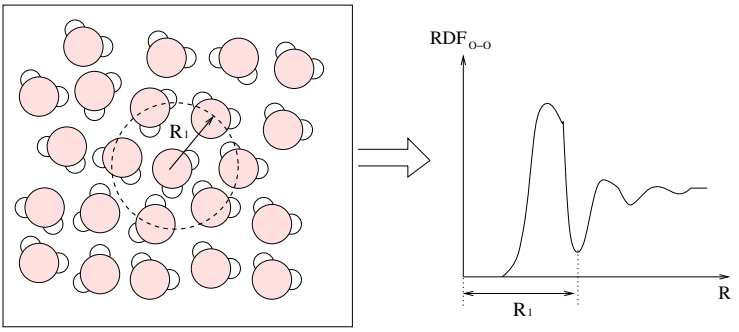

FIGURE 11.14. Schematic of bulk water molecules and the definition of the first coordination shell.

molecules are said to form a hydrogen bond if their interaction energy is less than a certain threshold energy E^c_{HB}. In the geometric criterion, two water molecules are said to form a hydrogen bond if (a) the O−O distance is less than certain distance $\mathrm{r}^c_{\mathrm{HB}}$ and (b) the O−H$\cdots$O angle is less than a certain threshold angle θ^c_{HB}. The O−O distance and O−H$\cdots$O angle are usually referred to as hydrogen bond length (r_{HB}) and hydrogen bond angle (θ_{HB}). Typically, E^c_{HB} is chosen to be -10 kJ/mol, $\mathrm{r}^c_{\mathrm{HB}}$ is chosen to be the radius of the *first coordination shell* of a water molecule, and θ^c_{HB} is chosen to be 30°. The first coordination shell of a water molecule is defined as the first water shell around that water molecule. The radius of the shell, R_1, is usually chosen to be the position of the first minimum of the oxygen–oxygen radial distribution function ($\mathrm{RDF}_{\mathrm{O-O}}$) (see Figure 11.14).

At the molecular level, the water structure is determined by the hydrogen bonding (HB) network. Since HB plays an important role in determining

the transport properties of water molecules and ions, it is important to understand how the HB network is influenced when the water is confined in nanochannels. The HB of water inside slit pores (Galle and Vortler, 1999; Galle and Vortler, 2001) and cylindrical pores (Allen et al., 1999; Rovere and Gallo, 2003; Walther et al., 2001a; Rovere et al., 1998; Werder et al., 2001; Spohr et al., 1999; Mashl et al., 2003) has been studied extensively in the past decades.

Figure 11.15 shows the number of hydrogen bonds per water molecule in a cylindrical pore as a function of the pore radius and surface properties (Allen et al., 1999). For a hydrophobic pore, the extent of HB is maximized at moderate radii ($r \approx 3.6$ Å), and drops notably as the pore size decreases. Similar observations have been reported for other hydrophobic pores, e.g., inside a carbon nanotube (Mashl et al., 2003). For a hydrophilic pore, the number of hydrogen bonds per water molecule is not sensitive to the pore size. However, if we exclude the hydrogen bonds between wall atoms and water molecule (dash-dot-dot curve in Figure 11.15), i.e., by counting only the hydrogen bonds between water molecules inside the pore, we find that the average number of hydrogen bonds per water molecule is significantly lower than that for the corresponding hydrophobic pores. This is because the water molecules inside the pore sacrifice water–water hydrogen bonds for the water–wall hydrogen bonds. Since the wall atoms are fixed, the strong interactions between water molecules and the wall atoms are likely to result in a reduced transport (e.g., diffusion transport) of water molecules in a hydrophilic pore compared to that in a hydrophobic pore.

(Rovere et al., 1998) also reported on the HB of water molecules inside a 4.0 nm diameter cylindrical SiO_2 pore. Figure 11.16 shows the number of hydrogen bonds as a function of distance from the center of the pore computed as the wall–water interactions are turned "on" (solid line) and "off" (dash line). Note that the number of hydrogen bonds decreases almost monotonically as we approach the pore surface when the wall–water interaction is turned on. However, when the surface atom–water interaction is turned off, the number of hydrogen bonds is essentially constant up to 15 Å from the pore center. Comparison of these two results indicates that the pure geometrical confinement can alone be responsible for the reduction in the number of hydrogen bonds at the interface.

Finally, the dynamic properties of HB have also been investigated. (Hummer et al., 2001) investigated HB inside a carbon nanotube of 8.1 Å diameter. They found that the HB inside the carbon nanotube is much more stable and highly oriented compared to that in the bulk. For example, the average lifetime of a hydrogen bond inside a carbon nanotube is 5.6 ps, compared to 1.0 ps in the bulk. In addition, less than 15% of the H–O$\cdots$H angles inside the carbon nanotube exceeds 30°, compared to 30% in the bulk. It was also reported that the OH bonds involved in the hydrogen bonds are nearly aligned with the nanotube axis, collectively flipping direction every 2 to 3 ns on average. In summary, the HB can be significantly

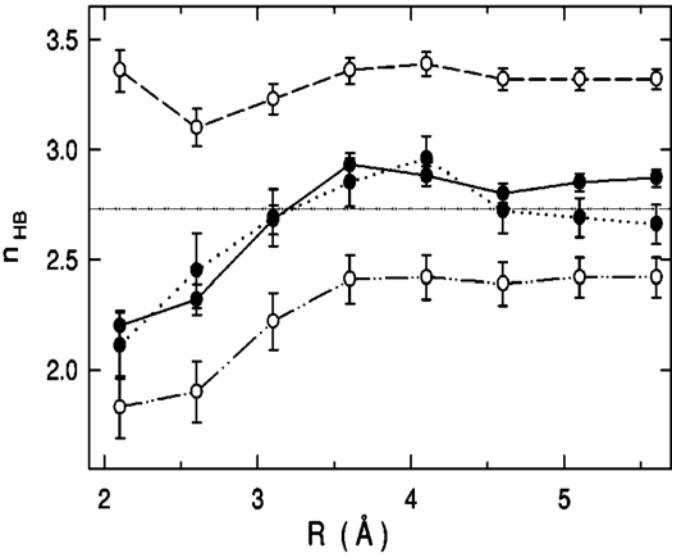

FIGURE 11.15. The effect of pore radius on the number of hydrogen bonds per water molecule for atomic hydrophobic (solid curve, filled circles), LJ hydrophobic (dotted curves, filled circles), and hydrophilic channels (dashed curve, open circles). The number of hydrogen bonds in hydrophilic pores when channel wall molecules are excluded are drawn as dash-dot-dot curves (open circles). (Courtesy of S.-H. Chung.)

influenced by the strong confinement inside a carbon nanotube, and the strongly stable hydrogen bonding inside the nanotube can change the wetting characteristic of the nanotube significantly (Hummer et al., 2001).

11.2.3 Contact Angle

The contact angle θ is a quantitative measure of the wetting of a solid by a liquid, as we have seen in Section 8.1; see Figure 8.4. At nanoscales, where the surface to volume ratio of the system can be orders of magnitude larger compared to a macroscopic system, the surface–water interactions tend to dominate the behavior of water in the system. The contact angle of water on the surface is a very important indicator of the strength of the surface–water interactions. Several authors have investigated the static wetting behavior of water on a graphite sheet (Werder et al., 2003) and on a carbon nanotube surface (Werder et al., 2001) and computed the contact angle of water on these surfaces.

(Werder et al., 2003) presented a study on the contact angle of water on a graphite surface by using molecular dynamics simulations. Figure 11.17

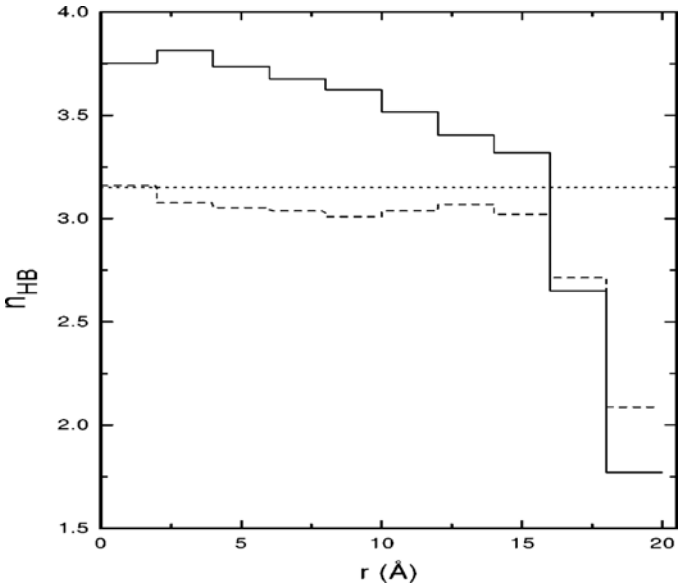

FIGURE 11.16. Number of hydrogen bonds as a function of the distance from the center of the pore, calculated with the wall–water interaction turned on (solid line) and off (dashed line). The horizontal dotted line represents the density-weighted average value of number of hydrogen bonds for confined water with the wall–water interaction turned on. (Courtesy of M. Rovere.)

shows snapshots of the system. It shows that a cubic water block will spontaneously evolve to a hemisphere as it reaches equilibrium. The contact angle of the water droplet on the graphite surface is a function of the Lennard–Jones potential between the carbon atom and the water molecule. The authors found that using a $\sigma_{CO} = 3.19$ Å and $\epsilon_{CO} = 0.392$ kJ/mol, one can reproduce the contact angle (86°) of water on a graphite surface as measured at the macroscopic scale. Such interaction parameters can then be very useful in the study of water behavior in carbon nanotubes.

Recently, (Gonnet et al., 2004) have suggested that the contact angle decreases weakly with increasing concentration of impurities like ions in water, and that chemisorption[1] of water onto the graphite surface, altering the partial charge distribution on the graphite surface, can influence the contact angle significantly.

[1] *Chemisorption*, or *chemical adsorption*, is adsorption in which the forces involved are valence forces of the same kind as those operating in the formation of chemical compounds, and the elementary step in chemisorption often involves an activation energy.

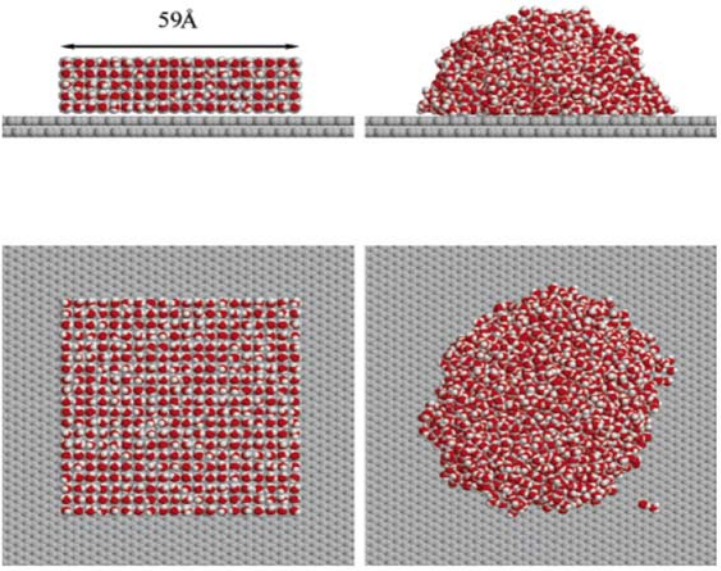

FIGURE 11.17. Side (top row) and top view (bottom row) of the initial ($t = 0$) and equilibrated ($t = 0.2$ ns) water droplet. The lateral graphite dimensions in the simulation are 119 Å ×118 Å. (Courtesy of P. Koumoutsakos.)

11.2.4 Dielectric Constant

From the results presented in this section, we can conclude that confinement can change the dipole orientation of water molecules significantly. This could lead to a change in the dielectric constant of water, which, in turn, can influence the dynamic properties and the electrostatic interactions between water molecules and between ion and water molecules. (Senapati and Chandra, 2001) studied the dielectric constant of water inside spherical cavities of various sizes using two different water models, namely, soft sticky dipole (SSD) (Liu and Ichiye, 1996) and SPC/E (Berendsen et al., 1987) models (see Section 11.1 for details). Figure 11.18 shows the dielectric constant computed using the two models as a function of the cavity size (Senapati and Chandra, 2001). Clearly, the dielectric constant in a nanocavity is significantly different from that in the bulk, and it decreases as the cavity radius decreases. Specifically, a nearly 50% decrease of the dielectric constant is observed in a cavity of about 12 Å diameter. Since the cavity surface is not charged, the reduction of the dielectric constant is purely an effect of confinement.

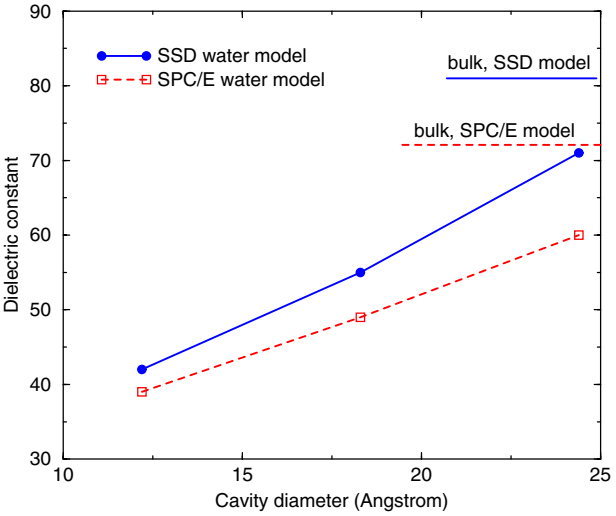

FIGURE 11.18. Dielectric constant of water confined in nanocavities of different cross sections. (Courtesy of A. Chandra.)

11.3 Dynamic Behavior

Understanding the dynamic behavior of water is critical to many biological and engineering applications. For example, the study of the diffusion of water molecules through nanochannels can help explain the operating mechanisms of the water channels, which are responsible for many important biological processes in the cell (Sui et al., 2001; Hummer et al., 2001; Beckstein and Sansom, 2003). In this section, we first review the research on the basic concepts of dynamic behavior of water and then summarize some of the simulation results on the diffusion transport of water through nanochannels. Finally, the filling and emptying kinetics of water in nanopores is discussed.

11.3.1 Basic Concepts

In this section, we focus our attention on the properties of the motion of a single water molecule in confined states, such as the reorientation dynamics, residence time, dipole correlation, and the velocity distribution. Understanding these properties can provide insight into the dynamic properties of water in more complicated scenarios such as the diffusion transport.

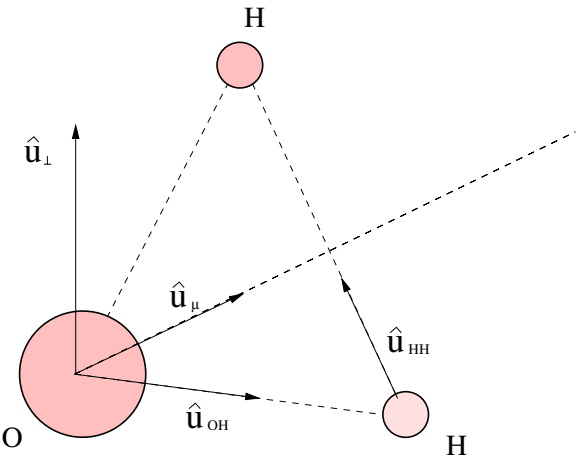

FIGURE 11.19. Definition of molecular unit vectors in a water molecule.

Reorientation Dynamics

Molecular reorientational motions in liquids are usually analyzed through the time correlation functions

$$C_{l,\alpha}(t) = \langle P_l(\hat{\boldsymbol{u}}_\alpha(t) \cdot \hat{\boldsymbol{u}}_\alpha(0)) \rangle \,,$$

where P_l refers to lth Legendre polynomial and $\hat{\boldsymbol{u}}_\alpha$ is a unit vector along a given direction ($\alpha = \mu$, HH, OH, $\perp$). As shown in Figure 11.19, four different unit vectors are considered: a unit vector $\hat{\boldsymbol{u}}_\mu(t) \equiv \boldsymbol{\mu}(t)/\mu(t)$ along the molecular dipole moment direction, a unit vector $\hat{\boldsymbol{u}}_{\mathrm{HH}}(t) \equiv \boldsymbol{r}_{\mathrm{HH}}(t)/r_{\mathrm{HH}}(t)$ along the H-H direction, a unit vector $\hat{\boldsymbol{u}}_{\mathrm{OH}}(t) \equiv \boldsymbol{r}_{\mathrm{OH}}(t)/r_{\mathrm{OH}}(t)$ along the O-H direction, and a unit vector $\hat{\boldsymbol{u}}_\perp(t) = \hat{\boldsymbol{u}}_\mu(t) \times \hat{\boldsymbol{u}}_{\mathrm{HH}}(t)$ perpendicular to the molecular plane. The correlation functions associated with the Legendre polynomials are

$$C_{1,\alpha}(t) = \langle \cos\theta_\alpha(t) \rangle \,,$$

$$C_{2,\alpha}(t) = \frac{1}{2} \left\langle \cos^2\theta_\alpha(t) - 1 \right\rangle ,$$

where $\cos\theta_\alpha \equiv \hat{\boldsymbol{u}}_\alpha(t) \cdot \hat{\boldsymbol{u}}_\alpha(0)$. The characteristic reorientational times $(\tau_1^\alpha, \tau_2^\alpha)$ are computed by

$$\tau_i^\alpha = \int_0^\infty C_{i,\alpha}(t)\, dt, \qquad (i = 1, 2)$$

The reorientational motion of water molecules is characterized by the dipole moment reorientation time $\tau_{1,2}^\mu$ (Martí et al., 2002). A smaller τ corresponds to a faster reorientation motion of the water molecule. Martí

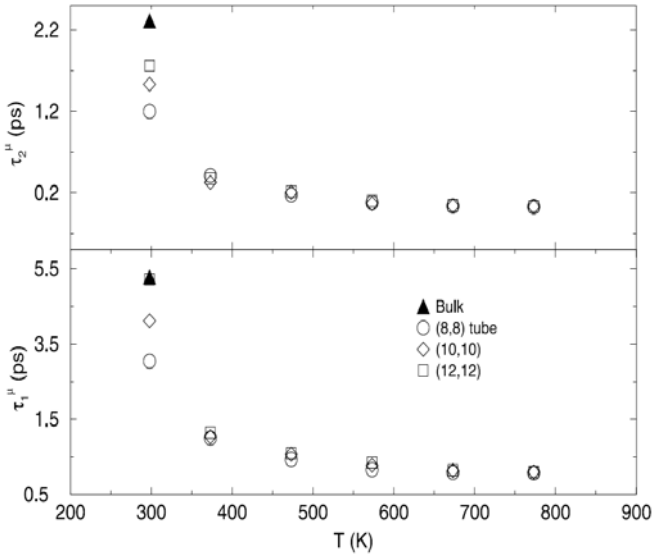

FIGURE 11.20. Molecular dipole moment reorientation time $\tau_{1,2}^{\mu}$ as a function of temperature at a density of 0.83 g/cm^3. Computation with the first (bottom) and second (top) Legendre polynomials. (Courtesy of J. Martí.)

and coworkers (Martí et al., 2002) studied the reorientation time of water molecules confined in carbon nanotubes of length 7.45 nm and internal radii of 2.65 Å ((8, 8) nanotube), 4 Å ((10, 10) nanotube) and 5.33 Å ((12, 12) nanotube); see Section 13.2.1 for details on carbon nanotubes. Figure 11.20 shows the reorientation time of the water dipole moment at different temperatures and in different-sized nanotubes. At room temperature, the smaller the nanotube diameter, the faster the reorientational motion, and in the largest nanotube, the reorientation time approaches that of the bulk water. From this result we can conclude that confinement tends to speed up molecular reorientations. The faster reorientational motion in small diameter nanotubes can be attributed to the partial breakdown of the tetrahedral hydrogen-bond network, which is typical when water is confined.

Residence Time

The mean time spent by a water molecule in its first coordination shell (see Section 11.2.2 for the definition) can be characterized by a residence time function $C_{\text{res}}(t)$. The spatial distribution of various molecules and ions closely surrounding a water molecule forms the coordinate shells of the water molecule. The first coordination shell gives rise to a noticeable

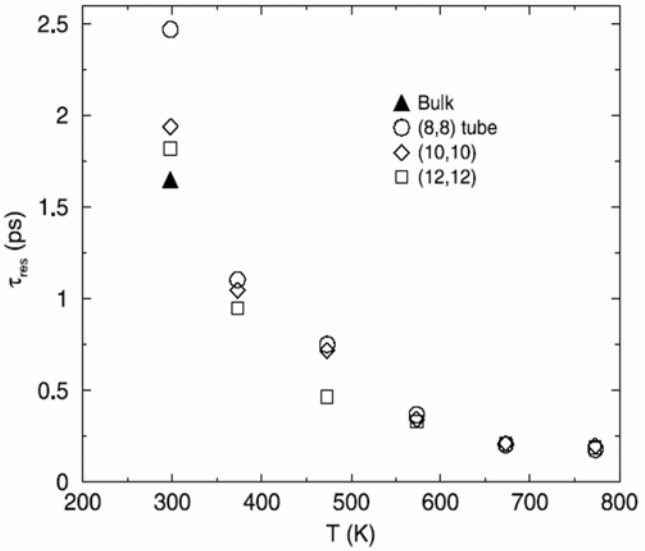

FIGURE 11.21. Residence time τ_{res} of a water molecule in its first coordination shell as a function of temperature in different-sized nanotubes at a density of 0.83 g/cm^3. (Courtesy of J. Martí.)

cluster, whereas the second coordination shell is more diffuse, and it becomes difficult to discern a pattern for subsequent coordination shells. The residence time for a given water molecule is defined as the number of water molecules in the first coordination shell of the tagged molecule during the time interval of length t. Usually, an exponential-like behavior of $C_{\text{res}}(t)$ is observed, and a residence time τ_{res} can be obtained from the fitting of $C_{\text{res}}(t)$ to a single exponential:

$$C_{\text{res}}(t) \approx c\, e^{-t/\tau_{\text{res}}}.$$

A longer residence time suggests that water molecules form a more stable structure. Figure 11.21 (Martí et al., 2002) shows the residence time τ_{res} of a water molecule in its first coordination shell as a function of the temperature in different-sized nanotubes. We observe that at room temperature, the residence time τ_{res} increases as the nanotube diameter decreases, indicating that a water molecule inside a narrow pore will spend longer time in its neighborhood than in larger pores. As the temperature increases, the residence time decreases sharply, and the deviation of τ_{res} in different-sized tubes also decreases.

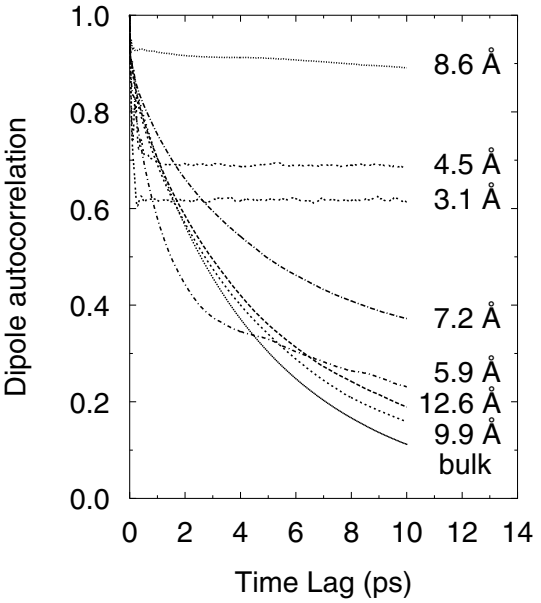

FIGURE 11.22. Water dipole correlation function inside nanotubes at 300 K.

Dipole Correlation

The reorientability of the water molecules can also be characterized by an autocorrelation function (ACF) of the water dipoles. The ACF is defined as

$$C(t) = \langle \boldsymbol{\mu}(0) \cdot \boldsymbol{\mu}(t) \rangle / \langle \mu^2 \rangle,$$

where $\boldsymbol{\mu}$ is the water dipole and the angle bracket denotes average over time and molecules. The reorientability of the water molecules plays an important role in determining the dynamic properties of water (e.g., viscosity, diffusivity).

(Mashl et al., 2003) studied the reorientability of the water molecules inside carbon nanotubes; Figure 11.22 shows the ACF obtained for water inside carbon nanotubes of various diameters. It was observed that for water in wide nanotubes, the ACFs generally take a bulk-like character. However, for smaller nanotubes, the appearance of a plateau suggests that the hydrogen bonds tend to form very rapidly and can be maintained for a much longer time compared to those in the bulk. An interesting observation is that the water molecules in the 8.6-Å nanotube show the largest degree of rotational immobilization, while the ACF of water molecules inside nanotubes that are slightly narrower or wider shows almost bulk-like behavior.

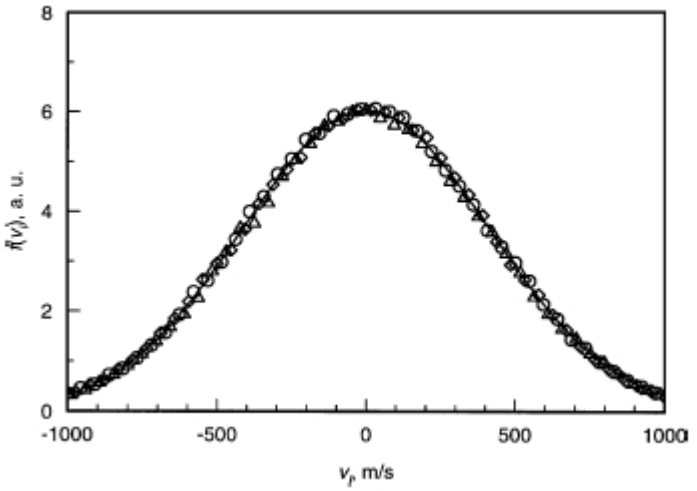

FIGURE 11.23. The distribution of the x- (circles), y- (triangles) and z-components (rhombi) of the translational velocities of water molecules at steady state. The solid line corresponds to the Boltzmann–Maxwell distribution. (Courtesy of J. Fischer.)

Velocity Distribution Function

The velocity distribution of water at a given temperature is a fundamental property, and in bulk it follows the Boltzmann–Maxwell distribution. However, whether water confined in a nanochannel would still obey the same velocity distribution is not that obvious. (Lishchuk and Fischer, 2001) studied the velocity distribution function of water confined in a 2.06 nm wide slit pore under an external microwave electric field. Figure 11.23 shows the distribution of the x-, y- and z-components of the velocity of water inside a 2.06 nm slit pore. It is observed that the velocity distribution obtained from the simulation agrees very well with the classical Boltzmann–Maxwell distribution.

11.3.2 Diffusion Transport

One of the motivations to study water behavior at nanoscale is to understand how its transport is influenced by confinement. Since diffusion is usually the dominant transport mechanism at small scales, the diffusion of water in nanochannels has been explored in detail in the past. Several researchers have investigated the diffusion of water inside artificial cylindrical nanopores (Allen et al., 1999; Lynden-Bell and Rasaiah, 1996; Zhou et al., 2003), inside silica nanopores (Rovere and Gallo, 2003; Spohr et al.,

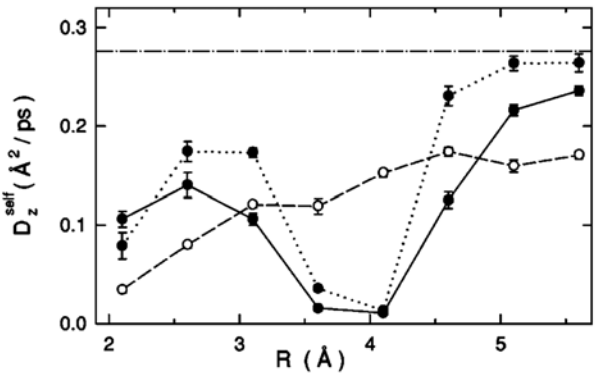

FIGURE 11.24. Self-diffusion coefficient along the axial direction (z-direction) of water molecules inside atomic hydrophobic (solid curve, filled circles), LJ hydrophobic (dotted curve, filled circles), and hydrophilic (dashed curve, open circles) pores. The horizontal dash-dot line is the bulk reference value. (Courtesy of S.-H. Chung.)

1999; Gallo et al., 1999), inside carbon nanotubes (Leo and Maranon, 2003; Mashl et al., 2003; Paul and Chandra, 2003), and inside slit nanopores (Brovchenko et al., 2001; Zhang et al., 2002).

(Allen et al., 1999) investigated the diffusion coefficient of water molecules inside artificial cylindrical pores of various radii and surface properties. Figure 11.24 shows the variation of the axial diffusion coefficient of water with the radii of the pore for atomic hydrophobic, LJ hydrophobic, and hydrophilic channels (see Section 11.2.1 for details on these channels). The result indicates that the axial (z-direction) self-diffusion of water molecules within hydrophobic pores experiences a dramatic fall for channel sizes with a radius of 3.6 to 4.1 Å. For a pore with a radius of 4.1 Å, the axial diffusion decreases to about 4% of the bulk value. This is mainly caused by the stable hydrogen-bonding network. As the pore size increases, the diffusion coefficient of water approaches its bulk value. It was also observed that the axial diffusion coefficient of water molecules inside a hydrophilic pore increases monotonically with the increase in the pore radius. The results also show that inside a small ($R < 3.0$ Å) or a large ($R > 5.0$ Å) pore, the water diffusion in a hydrophilic pore is slower than that in a hydrophobic pore. This can be explained by the preferred dipole orientation of the water molecules with the stationary wall molecules.

(Mashl et al., 2003) studied the diffusion of water inside carbon nanotubes with different diameters. Figure 11.25 shows snapshots of the system studied, and Figure 11.26 shows the mean-square displacement and axial diffusion coefficient of water molecules obtained inside different-sized nanotubes. Similar to the studies in (Allen et al., 1999), the water molecules

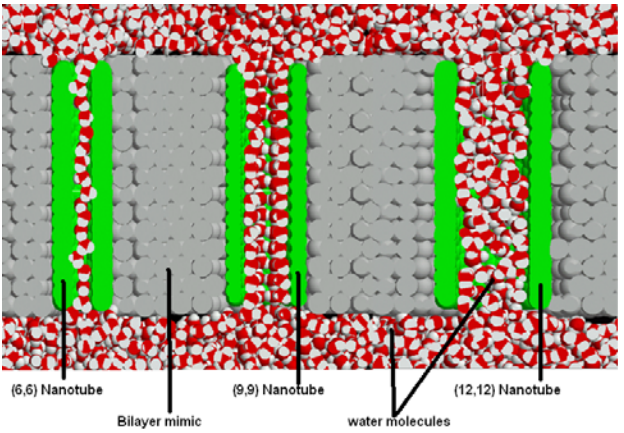

FIGURE 11.25. Snapshots from molecular dynamics simulations at 300 K with a composite image of three typical systems with nanotube size increasing from left to right. In narrow nanotubes (left), the water adopts a single-file arrangement with a 1-D hydrogen bonding but becomes more disordered in a fashion similar to that of bulk water in wider nanotubes (right). Confined within a nanotube of a "critical" diameter (center), the water spontaneously orders itself into a regular array with a 2-D hydrogen bonding.

are "immobilized" in a nanotube of 8.6 Å diameter. Panel (b) of Figure 11.25 shows the cross-sectional view of water structure inside the critically sized 8.6-Å-diameter nanotube. A stable hydrogen-bonding network is observed as expected. This is consistent with the diffusion coefficient results. Since the simulations were performed at 300 K, these results indicate that when the water is confined in a critical-diameter pore, it can behave in an ice-like manner even at room temperature. Such an effect can be very useful for a number of applications, such as proton conduction in synthetic ion channels.

11.3.3 Filling and Emptying Kinetics

In nanopores, confinement of the water can induce the so-called *drying transition* as a result of the strong hydrogen bonding between water molecules. This state can cause the water molecules to recede from the nonpolar surface to form a vapor layer separating the bulk phase from the surface (Stillinger, 1973; Lum et al., 1999; Lum and Luzar, 1997). This water behavior is important in understanding many biological processes, e.g., ion and water transport in biological channels where the channel dimension is of order a few angstroms and the channel surface is usually hydrophobic (Hummer et al., 2001). Motivated by the design of robust artificial ion and water chan-

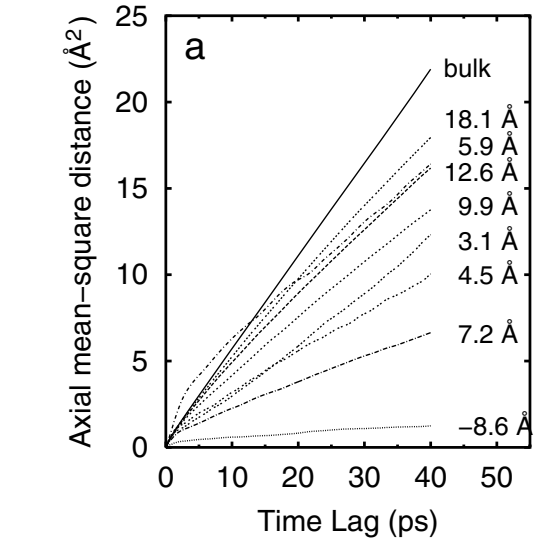

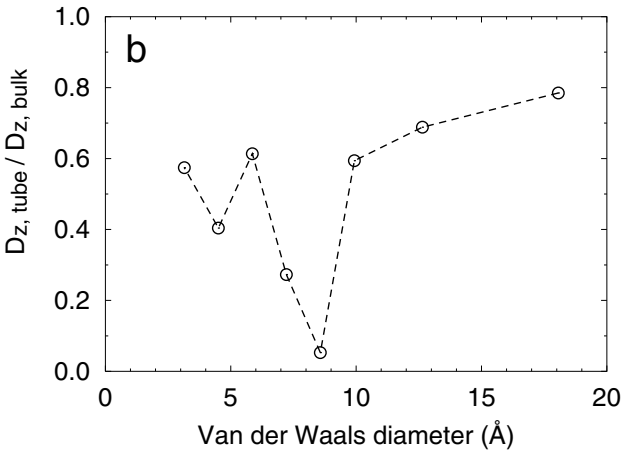

FIGURE 11.26. Water mobility inside nanotubes at 300 K. (a) Mean-square displacement (MSD) of water traveling along the nanotube axis for various nanotubes. (b) Axial diffusion coefficient of water, normalized to bulk (2.69×10^{-5} cm^2/s is the bulk value with SPC/E water), derived from panel (a).

nels (see Section 13.2 for more details on artificial ion channels), a number of researchers have investigated the filling and emptying of water in carbon nanotubes (Hummer et al., 2001; Waghe et al., 2002; Berezhkovskii and Hummer, 2002; Mann and Halls, 2003) and artificial nanopores (Allen et al., 2002; Beckstein and Sansom, 2003; Allen et al., 2003; Beckstein et al.,

2001; Kalko et al., 1995).

Water Entry in Hydrophobic Nanopores

Simulations of water conduction through carbon nanotubes (Hummer et al., 2001) indicate that even though nanotubes are hydrophobic, the channel has a steady occupancy of water molecules during the course of the simulation (Figure 11.27). Even for a 60-ns simulation (Hummer et al., 2001), the occupancies are not different. As mentioned in Section 11.2.2, the high occupancy of water inside the hydrophobic nanotube is mainly caused by the stable hydrogen bond inside the nanotube. (Hummer et al., 2001) explained this quantitatively by computing the local excess chemical potential, $\mu_{\mathrm{NT}}^{\mathrm{ex}}$, defined as the negative free energy of removing a water molecule from the channel. Such a free energy is not dominated by how strongly bound a water molecule is on average, but by how populated weakly bound states are. Even though the binding energy of water molecules inside the nanotube is unfavorable compared to bulk water, the binding energy inside the nanotube is more sharply distributed (see Figure 11.28), and high-energy states dominating the free energy are less frequently occupied. As a result, though the water molecules inside the nanotube lose about 2 kcal/mol in energy, they have a lower excess chemical potential of $\mu_{\mathrm{NT}}^{\mathrm{ex}} \approx -6.87 \pm 0.07$ kcal/mol, compared to bulk water of $\mu_{\mathrm{NT}}^{\mathrm{ex}} \approx -6.05 \pm 0.02$ kcal/mol. Water molecules not only penetrate the nanotube, but they also transport across the nanotube, and on average, about 17 water molecules pass through the nanotube per nanosecond (see Figure 11.29). The conduction occurs in a burst-like manner because of the tight hydrogen-bonding network inside the nanotube; rupturing the water chain is energetically costly, and so rare. However, once the rupture of the hydrogen bond occurs, the water chain moves with little resistance through the nanotube, resulting in a burst of the water flow.

Filling Mechanism

When the diameter of the nanopore is small enough for a single-file chain (in a single-file chain the water molecules move as a single chain), the mechanism of filling the nanopore can be understood as summarized below (Waghe et al., 2002):

1. Filling of water molecules in a nanopore can occur from either side of the nanopore, with hydrogens entering first, dipoles oriented outward.

2. Filling of water molecules progresses as a chain from the end; it is initiated with the orientation remaining the same.

3. Simultaneous filling from both sides is not favorable, because the dipole orientations at the ends repel each other.

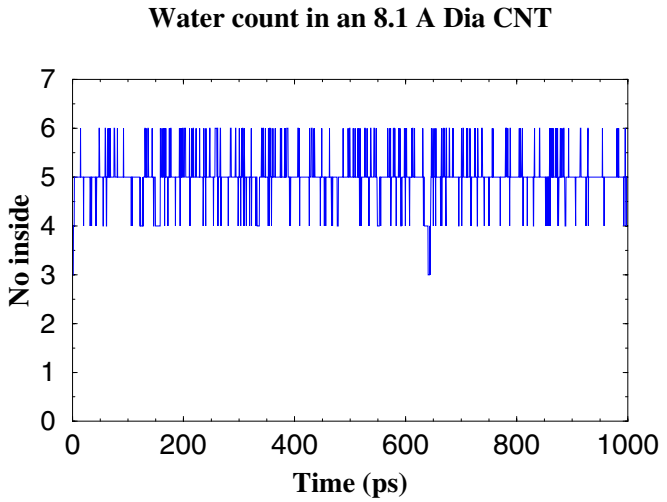

FIGURE 11.27. Water occupancy: number of water molecules inside the nanotube as a function of time.

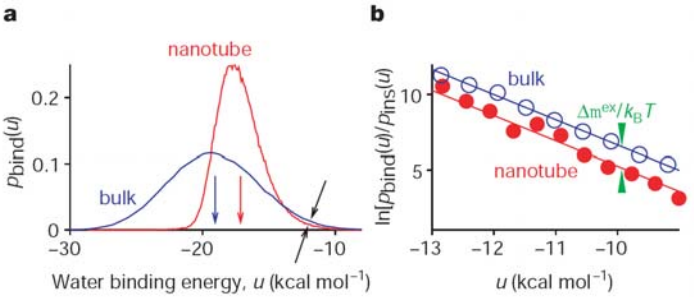

FIGURE 11.28. Water binding energies. ***a.*** Probability density $p_{\mathrm{bind}}(u)$ of binding energies u for bulk water and water inside the nanotube. Vertical arrows indicate average binding energies. Tilted arrows indicate crossover region, in which weakly bound states are more populated in bulk water. ***b.*** $\ln[p_{\mathrm{int}}(u)/p_{\mathrm{ins}}(u)]$ for water inside the nanotube and in bulk TIP3P water (open circles), fitted to $\beta(\mu_w^{\mathrm{ex}} - u)$ (lines). The vertical distance between the two parallel lines of slope $-\beta$ gives the difference in the excess chemical potentials, $\beta(\mu_w^{\mathrm{ex}} - \mu_{\mathrm{NT}}^{\mathrm{ex}})$. (Courtesy of G. Hummer.)

4. Depending on the material (wall)–oxygen van der Waal's interaction forces, the chain can rupture at the ends, causing conduction in bursts as in carbon nanotubes or stable as in silicon dioxide pores.

5. Filling and emptying occurs mainly by the sequential addition of wa-

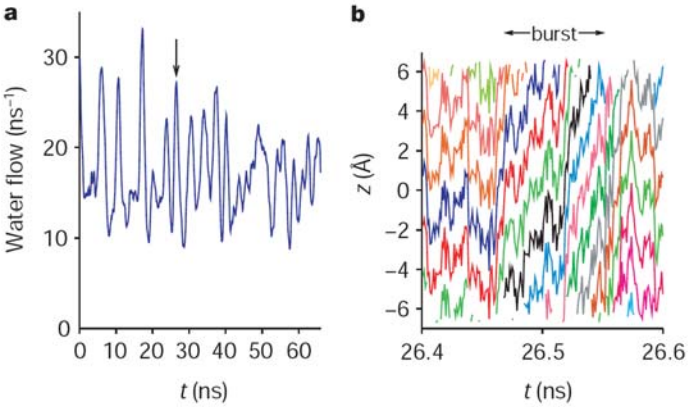

FIGURE 11.29. Water flow through the nanotube. ***a.*** Numbering of water molecules leaving the nanotube at time t that entered the nanotube from the other side. Individual water conduction events are smoothed with a 1-ns-wide triangular filter. ***b.*** motion (along the tube length) of individual water molecules during the conduction "burst" at 26.5 ns. (Courtesy of G. Hummer.)

ter to or removal from the single-file water chain inside the nanotube.

Figure 11.30 shows the trajectories of individual water molecules entering a silicon dioxide nanopore about 8 Å in diameter and 6 nm long as a function of time. With longer tubes, the dipoles at the ends do not repel each other as much as in a shorter tube, so chains form at both ends. But one of them becomes dominant, and then filling progresses sequentially through that chain till the chains meet. Figure 11.31 shows the filling as distributions of normalized dipole orientations of water molecules with respect to the axis of the tube. Here the behavior of water with respect to time does not come into the picture, but rather the fact that orientation remains the same in a chain. The orientations are predominantly either -1 or $+1$, showing that the direction of entry is along the axis of the tube from either end.

Sensitivity to Water–Nanotube Interaction Parameters

The simulations performed on different types of nanotubes show that the water entry is highly sensitive to the interaction of water with the nanotube. A small reduction of the attraction between the carbon nanotube and the water changes the hydration of the nanotube dramatically, and a sharp two-state transition between empty and filled states on a nanosecond time scale occurs in the nanopores (Waghe et al., 2002; Hummer et al., 2001; Beckstein et al., 2001). Table 11.4 summarizes the LJ parameters from various papers, all agreeing the fact that above a particular value of $\sigma_{\text{oxygen}-\text{wall}}$, the tube

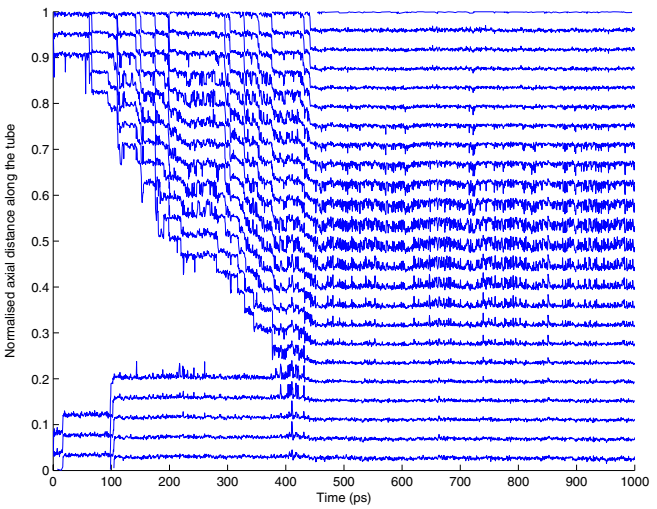

FIGURE 11.30. Trajectories of individual water molecules in a nanopore in a silicon dioxide membrane 8 Å in diameter and 6 nm long.

is empty.

Sensitivity to Nanotube Radius and Partial Charges on the Wall

(Allen et al., 2003) studied the filling and emptying in an artificial ion channel with varying diameter and different permittivities of the membrane surrounding the channel. They found that the permeation of a pore of fixed length is very sensitive to the pore radius. For very narrow pores ($R < 0.55$ nm in their simulations), water molecules are excluded from the pore. As the pore radius increases to a threshold value ($R = 0.60$ nm when the permittivities of the membrane is 1.0), intermittent permeation occurs, and the pore fluctuates between the "filled" and "empty" states stochastically. Further increase of the pore radius (e.g., $R > 0.65$ nm) then leads to the complete filling of the pore. The threshold radius is sensitive to the permittivity of the channel membrane, and using a polarizable membrane results in a decreased threshold radius for the intermittent permeation. In contrast to what was reported for a small carbon nanotube, where the water filled in the nanotube forms a one-dimensional chain, the authors found that the filled channel contains a much larger number of water molecules, and these water molecules exhibit a bulk-like behavior. Such a difference is mainly caused by the different properties of the pore surface. The simulations also reveal that the filling process is preceded by formation of a percolating chain of water molecules through the nanopore (see Figure 11.32), and the channel filling seems to "nucleate" around a percolating cluster. The proposed filling mechanism can be understood by

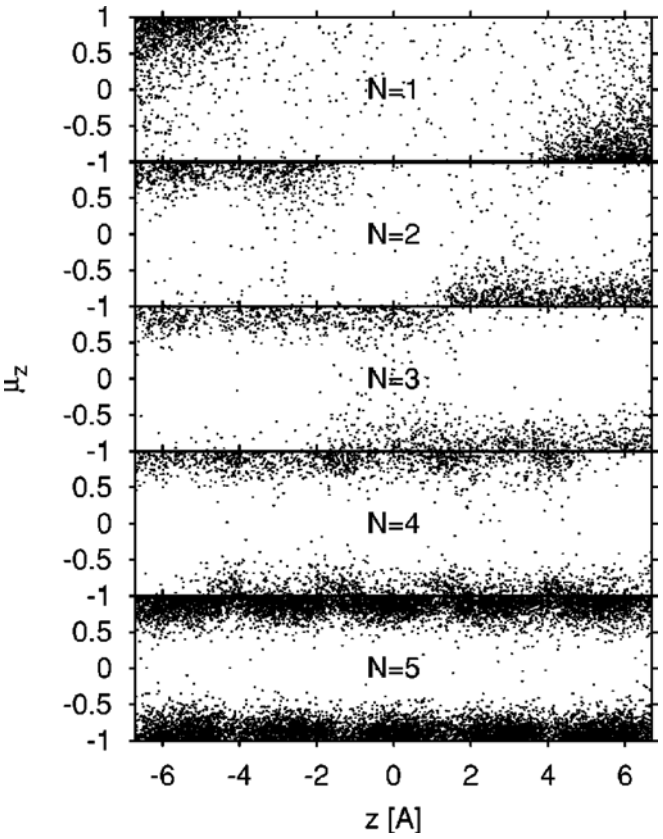

FIGURE 11.31. Normalized dipole of water molecules inside the tube projected onto the tube axis as a function of the position z of the water–oxygen atom along the tube axis. Each point corresponds to one water molecule in a saved configuration. The results are separated for $N = 1$ to 5 water molecules inside the tube (top to bottom). It was observed that for a single molecule in a tube, the water dipole moments point inward preferentially. With subsequent molecules entering into the tube, this orientational preference is maintained, such that the chain grows with all dipoles pointing inward. As a consequence, the dipolar orientations of water chains entering from the two ends simultaneously are not compatible, thus disfavoring simultaneous filling from both sides. (Courtesy of G. Hummer.)

analyzing Figure 11.33, where the average number of percolating chains in the channel is plotted as a function of the number of water molecules n inside the channel. Clearly, when n is small, there is never a percolating cluster, and when n is large enough, there is almost always one present. (Beckstein et al., 2001) show that the filling can be enhanced by placing dipoles along the walls of the nanotube at diameters at which water cannot enter the tube.

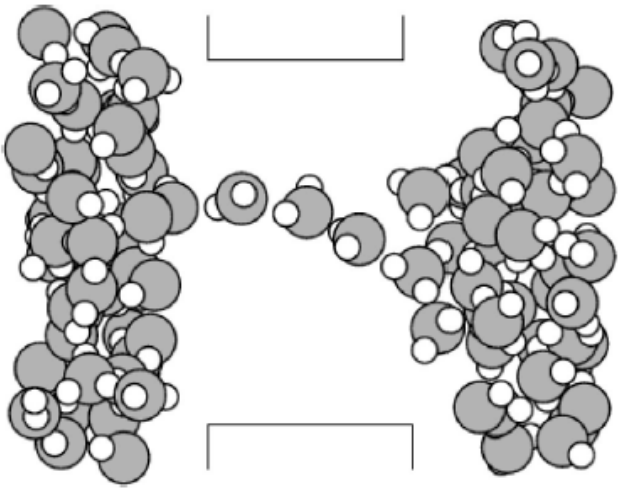

FIGURE 11.32. Snapshot of a "percolating cluster" from a biased simulation run with a pore radius of 0.6 nm and length of 0.8 nm. Only the water molecules near the pore are shown. The positions of the confining walls are indicated. (Courtesy of S. Melchionna.)

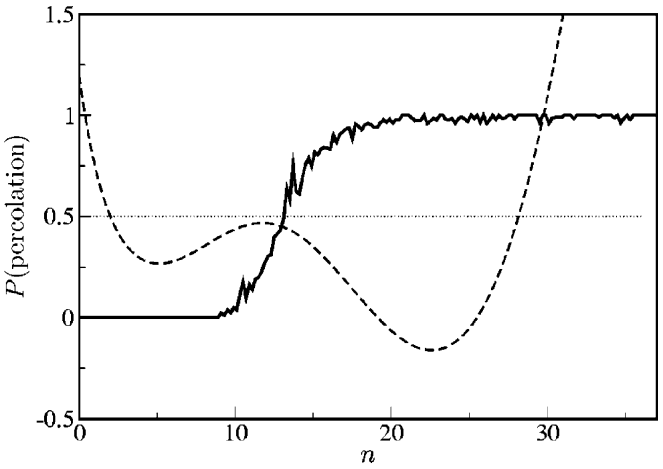

FIGURE 11.33. Probability of finding an unbroken chain of water molecules through the pore as a function of the water molecules inside the pore shown in Figure 11.32. The dashed line shows a scaled grand potential profile. (Courtesy of S. Melchionna.)

TABLE 11.4. Dependence of the full and empty states of water on the Lennard–Jones interaction parameters.

Nanotube material	Tube Diameter (Å)	Tube Length (Å)	$\sigma_{\text{oxygen}-\text{wall}}$ (Å)	Fill/Empty States
Artificial Membrane (Beckstein et al., 2001)	9.0	8.0	3.42	Both States
Carbon nanotube (Waghe et al., 2002)	8.1	27.0	3.27	Full
Carbon nanotube (Waghe et al., 2002)	8.1	27.0	3.41	Both States
Carbon nanotube (Waghe et al., 2002)	8.1	27.0	3.43	Empty
Carbon nanotube (Hummer et al., 2001)	8.1	13.4	3.23	Full
Artificial Slab	9.1	15.1	3.49	Both States
Silicon Dioxide	10.0	60.0	3.27(Si), 3.16 (O)	Full

Summary

In summary, from the various results presented in this chapter, we note that water in confined nanochannels can exhibit very interesting and different physical characteristics compared to that of bulk water. The properties of water in confined nanochannels can depend strongly on the type of surface (hydrophilic versus hydrophobic channel wall structure) and on whether the nanopore surface is charged. It is important to properly understand the merits and limitations of the various water models before they can be used for nanotechnology design.